Dimensional changes of metallic glasses during bombardment with fast heavy ions

Ming-dong Hou,* S. Klaumünzer, and G. Schumacher
Hahn-Meitner-Institut, Postfach 39 01 28, D-1000 Berlin 39, Germany
(Received 31 August 1989)

Small strips of various metal-metalloid glasses and metal-metal glasses have been irradiated below 50 K with 360-MeV Xe ions. Special care has been taken to achieve a rather uniform energy deposition throughout the samples. Projectile implantation has been avoided. Prior to and after irradiation, the macroscopic dimensions of the samples were determined at room temperature. Above an incubation fluence of a few 10^{12} Xe ions/cm^2 all glasses have shown drastic, irreversible changes in sample dimensions. Density measurements exclude swelling as a possible explanation and demonstrate that the dimensional changes are anisotropic. Each ion acts like a hammer, i.e., above the incubation fluence the sample dimensions perpendicular to the ion beam grow indefinitely with increasing fluence, whereas the sample dimension parallel to the beam shrinks. A control experiment with several crystalline metals (Al, Cu, Fe, Nb, Pt, W) and alloys ($Cu_{55}Zn_{45}$, $Cu_{70}Zn_{30}$, $Ni_{80}Cr_{20}$, $Ni_{90}Cr_{10}$, $Fe_{70}Cr_{25}Al_5$) reveals that the occurrence of the dimensional changes is closely related to the amorphous structure. The results are explained by a model, which assumes that the passage of an ion generates locally high mechanical stresses, which release shear transformations. Similarities and differences between the present model and the well-known ion-explosion-spike model are discussed and compared with the experimental data.

I. INTRODUCTION

Fast ions in matter lose their energy predominantly via two mechanisms. First, there is a direct transfer of kinetic energy to target atoms by elastic collisions between a projectile nucleus and target nuclei. This mechanism is commonly denoted as nuclear energy loss S_n. Energy is also transferred to target electrons by the generation of excited or ionized target atoms. This mechanism is called electronic energy loss S_e and contributes the most to the deceleration of fast ions of kinetic energy ≥ 1 MeV/u. For light ions the electron energy loss is relatively low, so that electronic excitations and ionizations are sparsely distributed along the ion's path. Hence, electronic relaxation processes necessarily reflect the specific electronic structure (band, excitons, excimers) of the target.[1-3] For fast heavy ions, however, the density of electronic excitations and ionizations becomes so high that new and collective effects arise.[1-3] Consequently, a reference to the near-equilibrium electronic structure is probably inadequate for the description of the electronic relaxation processes.

It has long been known that electronic excitations can provoke structural changes in materials, particularly in insulators. The understanding of the operative mechanisms, however, is quite incomplete[1-3] and, with respect to high-density electronic excitations, one has to resort to rather general concepts of which validity and applicability are not clear *a priori*. For example, the formation of nuclear tracks in insulators by electronic excitations and ionizations is frequently discussed within the model of the ion-explosion spike.[4] Although it provides a reasonable explantion for a variety of experimental observations, this model is certainly a naive approach to reality.[5] Therefore, further experimental work is required in order to test already existing models and to stimulate new calculations. In particular, with the rise of megavolt implanters in the semiconductor technology, a deeper understanding of the occurring electronic excitations, their relaxation paths, and the attendant atomic rearrangments is highly desirable.

Several years ago it was discovered[6,7] that the metallic glasses $Pd_{80}Si_{20}$ and $Cu_{50}Zr_{50}$ exhibited a peculiar behavior when subjected to bombardment with a beam of fast heavy ions. It was found that, with increasing fluence, the sample dimensions perpendicular to the ion beam grew indefinitely, whereas the sample dimension parallel to the ion beam shrank in such a way that the mass density remained virtually unaltered. Additional measurements of x-ray diffraction and electrical resistivity revealed that the structural modifications of the radiation-deformed samples were small in comparison to the dimensional changes.[6,7]

The discovery of this ion-beam-induced instability of glassy $Pd_{80}Si_{20}$ and $Cu_{50}Zr_{50}$ was very surprising with respect to three facts. (i) At that time there was the supposition[8] that a metallic glass, as a completely disordered metal, would be more radiation resistant than any crystalline metal. (ii) In the latter materials any radiation-induced anisotropic change in sample dimensions was due to a natural crystallographic anisotropy.[9] In sharp contrast, the anisotropy of the dimensional changes in glassy $Pd_{80}Si_{20}$ and $Cu_{50}Zr_{50}$ was introduced by the beam itself.[6,7] (iii) The number of atoms, which obviously occupied new positions in order to constitute the dimensional changes, exceeded by 1 or 2 orders of magnitude the number of atoms which are displaced via the nuclear energy loss.[6,7,10,11] These three unexpected facts found their solution when it was realized that the whole phenomenon was predominantly driven by the electronic

energy loss.[11–14] This experimental finding was in disagreement with the commonly accepted view that electronic excitation would be so rapidly and efficiently shared among the continuum states in the conduction band of metals that it would be neither spatially localized nor retained in sufficiently large units to produce atomic displacements.[1] Therefore, the radiation-induced dimensional instability of glassy metals provides a new access to the question concerning the way in which an intense electronic excitation can provoke atomic rearrangements in solids. Of course, in this context, a more comprehensive study of this phenomenon is of particular interest. In this paper we report on the experimental results of a large variety of metallic glasses which have been exposed at low temperatures to a beam of 360-MeV Xe ions. Preliminary results of this study have already been published in Refs. 10 and 15.

II. EXPERIMENTAL

A. Specimen preparation

The glassy materials were obtained from various suppliers in the form of ribbons with thicknesses ranging from 15 to 60 μm. Nominal compositions, mass densities, and original thicknesses t_r of the glassy ribbons are listed in Tables I and II for metal-metalloid and metal-metal glasses, respectively. By means of the PRAL algorithm[16] the projected ranges R_p and range stragglings ΔR_p of 360-MeV Xe ions were calculated for all materials. These results are also listed in Tables I and II.

Former experiments[6,7] had shown that a uniform energy deposition throughout the samples by the fast ions is a prerequisite to obtain clear-cut results. A first step toward a fulfillment of this condition was a considerable thickness reduction of the glassy ribbons by means of rolling at room temperature between stainless-steel rollers or hard metal rollers. The choice of the rollers used depended on the mechanical hardness of the ribbons. After rolling, in a few cases, additional electropolishing was applied to achieve a clean specimen surface. The final thickness t_0 of the samples that were used for the irradiation experiments is also included in Tables I and II. In most cases, t_0 was less than $0.6R_p$, i.e., projectile implantation was negligible.

In order to test the influence of cold rolling on the radiation-induced changes of dimensions, a subset of cold-rolled samples of the hard glasses $Fe_{80}B_{20}$, $Ni_{78}Si_8B_{14}$, and $Co_{75}Si_{15}B_{10}$ were annealed at 150 °C in argon atmosphere for 1 h. In a test irradiation it turned out, however, that the deformation during ion bombardment was fairly independent of the pretreatment of the samples. Therefore, in all subsequent irradiation runs the specimens were used in the cold-rolled state.

Small pieces of a rectangular shape (approximately 3×1 mm^2) were cut from the cold-rolled glasses. Five to six samples, differing in glass composition, were clamped side by side between two small copper plates so that a portion (approximately 0.8×1 mm^2) of each sample stood out and was thus available for exposure to the ion

TABLE I. List of the metal-metalloid glasses of this work together with their suppliers, mass densities D, and original ribbon thickness t_r. The ribbons were thinned to thickness t_0 considerably less than the projected ranges R_p of 360-MeV Xe ions. ΔR_p denotes the range straggling.

Alloy	Supplier	D (g/cm^3)	t_r (μm)	t_0 (μm)	$R_p\pm\Delta R_p$ (μm)
$Pd_{80}Si_{20}$	VAC	10.25[c]	38	6.7–8.5	12.0±0.5
$Pd_{84}Si_{16}$	a	10.67[c]	30	5.2–7.2	11.6±0.5
$Pd_{78}Fe_5Si_{17}$	a	10.36[c]	23	6.6–6.8	11.7±0.5
$Pd_{73}Fe_{10}Si_{17}$	a	10.16[c]	30	5.7–7.1	11.8±0.5
$Pd_{68}Fe_{15}Si_{17}$	a	9.94[c]	17	6.0–6.5	11.9±0.5
$Pd_{73}Co_{10}Si_{17}$	a	10.25[c]	23	6.0–7.2	11.8±0.5
$Pd_{68}Ni_{15}Si_{17}$	a	10.10[c]	30	6.7–7.5	11.8±0.5
$Fe_{80}B_{20}$	Allied Chemicals	7.40[d]	38	5.7–6.8	12.3±0.5
$Fe_{79}B_{16}Si_5$	Goodfellow	7.28[d]	20	6.0–7.0	12.4±0.5
$Fe_{78}B_{13}Si_9$	Goodfellow	7.18[d]	20	6.0–7.0	12.6±0.4
$Fe_{81}B_{13.5}Si_{3.5}C_2$	Goodfellow	7.32[d]	27	6.0–7.0	12.4±0.4
$Fe_{40}Ni_{40}B_{20}$	VAC	7.71[d]	45	5.7–7.1	12.1±0.4
$Fe_{40}Ni_{38}Mo_4B_{18}$	Goodfellow	7.90[d]	25	6.0–7.0	12.1±0.4
$Ni_{78}Si_8B_{14}$	VAC				
	Goodfellow	8.00[d]	37,25	5.8–7.5	12.0±0.4
$Co_{75}Si_{15}B_{10}$	VAC	7.73[d]	45	7.0–8.0	12.2±0.4
$Co_{66}Fe_4Mo_2B_{12}Si_{16}$	Goodfellow	7.70[d]	25	6.0–7.0	12.3±0.4
$Mo_{48}Rh_{32}B_{20}$	b	10.15[c]	15	6.0–7.0	11.7±0.5

[a]Alloy supplied by Dr. H. R. Khan, Forschungsinstitut für Edelmetalle, Schwäbisch Gmünd, Germany.
[b]Alloy supplied by Dr. J. Wecker, Institut für Metallphysik, Universität Göttingen, Germany.
[c]This work and P. H. Gaskell, Acta Metall. **29**, 1203 (1981).
[d]Data from data sheet of supplier.

TABLE II. Same as Table I but for the metal-metal glasses of this work. All glasses except $Cu_{64}Ti_{36}$, which was obtained from Vacuumschmelze VAC Hanau, Germany, were supplied by Dr. J. Wecker, Institut für Metallphysik, Universität Göttingen, Göttingen, Germany.

Alloy	D (g/cm^3)	t_r (μm)	t_0 (μm)	$R_p \pm \Delta R_p$ (μm)
$Be_{32.5}Zr_{67.5}$	5.69[a]	20	6.5±0.5	19.0±0.5
$Be_{32.5}Nb_7Zr_{60.5}$	5.83[a]	20	6.5	18.4±0.5
$Be_{32.5}Mo_7Zr_{60.5}$	6.00[a]	17	6.5	18.7±0.5
$Be_{40}Ti_{50}Zr_{10}$	4.13[b]	40	6.5	20.7±0.5
$Co_{22}Zr_{78}$	6.94[c]	19	6.5	15.9±0.5
$Cu_{35}Zr_{65}$	7.00[c]	24	6.5	15.9±0.5
$Ni_{24}Zr_{76}$	6.88[c]	21	6.5	16.0±0.5
$Fe_{22}Zr_{78}$	6.78[c]	15	6.5	16.2±0.5
$Fe_{33}Zr_{67}$	6.93[c]	15	6.5	15.5±0.5
$Fe_{40}Zr_{60}$	7.03[c]	15	6.5	15.1±0.4
$Fe_4Cu_{36}Zr_{60}$	7.07[c]	15	6.5	15.6±0.4
$Fe_8Cu_{32}Zr_{60}$	7.07[c]	18	6.5	15.6±0.4
$Fe_{16}Cu_{24}Zr_{60}$	7.08[c]	17	6.5	15.4±0.4
$Fe_{24}Cu_{16}Zr_{60}$	7.08[c]	19	6.5	15.3±0.4
$Cu_{64}Ti_{36}$	6.92[d]	60	6.5	14.4±0.5
$Cu_{43}Ti_{57}$	5.90[d]	18	6.5	16.0±0.5
$Nb_{40}Ni_{60}$	8.54[e]	18	6.5	12.3±0.4

[a]Calculated from data of R. Hasegawa and L. E. Tanner, J. Appl. Phys. **49**, 1196 (1978); Phys. Rev. B **16**, 3925 (1977).

[b]L. E. Tanner and R. Ray, Scr. Metall. **11**, 783 (1977).

[c]Calculated from data of Z. Altounian and J. O. Strom Olsen, Phys. Rev. B **27**, 4149 (1983); H. U. Krebs and J. C. Freyhardt, Ref. 10, p. 439; Z. Altounian, C. A. Volkert, and J. O. Strom Olsen, J. Appl. Phys. **57**, 1777 (1985).

[d]This work.

[e]E. Svab *et al.*, J. Non-Cryst. Solids **104**, 291 (1988); R. C. Ruhl, B. C. Giessen, M. Cohen, and N. J. Grant, Acta Metall. **15**, 1693 (1967); S. Basak, R. Clark, and S. R. Nagel, Phys. Rev. B **20**, 4278 (1979).

beam. An indium layer was placed between the two plates to ensure good thermal contact between the specimens and the sample holder. Several of these sample holders could be tightly screwed to a massive copper frame soldered with Wood's metal to the cold stage of a liquid-helium cryostat (see Fig. 1). Again an indium layer was used between the sample holders and the copper frame.

The total number of glassy samples irradiated amounted to about 180. No special effort was made to check the amorphicity of the samples, relying on the information of the suppliers. It should be noted, however, that a small crystalline fraction in an otherwise glassy matrix would probably not significantly change the experimental results since an integral quantity is measured. Moreover, crystalline particles of the investigated alloys are expected to rapidly amorphize by heavy-ion irradiation at low temperatures.[17,18]

In order to check whether the occurrence of ion-beam-induced dimensional changes is related to the amorphous structure, specimens of various crystalline metals and alloys were prepared similarly to those of the metallic glasses. All crystalline materials selected had a cubic crystal structure to avoid dimensional changes which might appear during irradiation due to a natural crystallographic anisotropy.[9] The purity of the metals and the nominal composition of the alloys are summarized in Table III, together with the specimen thickness

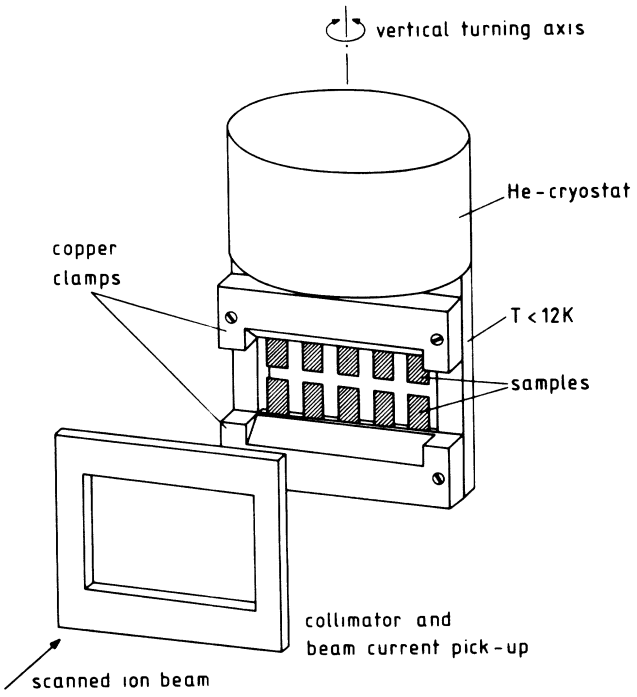

FIG. 1. Experimental apparatus for bombardment of glassy and crystalline samples with fast heavy ions at low temperatures.

TABLE III. Same as Table I but for the crystalline metals and alloys of this work.

Alloy	Supplier	D^c (g/cm^3)	t_0 (μm)	$R_p \pm \Delta R_p$ (μm)
Al (purity 99.99%)	Goodfellow	2.70	15.0±1.5	26.8±0.8
Cu (purity 99.97%)	Goodfellow	8.96	6.0±0.5	12.1±0.4
Fe (purity 99.85%)	Goodfellow	7.87	3.0±0.5	11.9±0.4
Nb (purity 99.90%)	Goodfellow	8.57	3.0±0.5	12.9±0.5
Pt (purity 99.95%)	Goodfellow	21.5	4.0±0.5	9.2±0.5
W (purity 99.95%)	Goodfellow	19.3	6.0±0.5	9.9±0.5
$Ni_{80}Cr_{20}$	Goodfellow	8.4	5.0±0.5	11.7±0.4
$Ni_{90}Cr_{10}$	Heraeus[a]	8.5	6.0±0.5	11.7±0.4
$Fe_{70}Cr_{25}Al_5$	Goodfellow[a]	7.1	6.5±0.5	13.0±0.4
$Cu_{55}Ni_{45}$	Goodfellow[a]	8.9	5.0±0.5	11.8±0.4
$Cu_{70}Zn_{30}$	b	8.55	6.2±0.5	12.7±0.5

[a]Cold-rolled from wire, no further annealing treatment.
[b]Material supplied by Dr. R. Poerschke, Its original thickness of 65 μm was reduced to 6.2 μm by cold rolling. In a subsequent annealing treatment (1 h) at 500 °C and additionally at 230 °C a reference equilibrium state of short-range order has been established [C. Abromeit and R. Poerschke, Radiat. Eff. **85**, 57 (1984)].
[c]Density data from supplier.

t_0 before irradiation, the projected range R_p, and the corresponding range straggling of 360-MeV Xe ions. The materials of Table III were used in the as-received state, unless a footnote indicates a special treatment.

B. Irradiation procedure

The liquid-helium cryostat was inserted into a special vacuum chamber mounted at the beam line of the VICKSI accelerator in Berlin. The cryostat could be turned *in situ* by ±180° around a vertical axis (Fig. 1), which enabled a rapid exchange of entrance and exit of the beam to the samples. In addition, the cryostat could be moved along the vertical axis for sample positioning. The proper irradiation position was determined by a telescope and checked during bombardment by the luminescence light emitted from a ceramic layer cemented onto the sample holders.

Only one irradiation geometry was used in this work, i.e., the surface normal of the samples was aligned parallel to the ion beam. Usually, five to twelve specimens were irradiated simultaneously (see Fig. 1) by sweeping the beam spot (typically 2–3 mm in diameter) horizontally (~500 Hz) and vertically (~23 Hz) in such a way that the opening (10×4.5 mm^2) of a beam collimator in front of the cryostat was homogeneously irradiated. The collimator consisted of four electrically insulated tantalum plates on which the striking beam produced electrical signals. These signals were used for both continuous beam intensity monitoring and determination of accumulated fluence, as well as for a feedback to an automatic beam-positioning control system. Between collimator and cryostat, a Faraday cup could be placed to calibrate the collimator signals by the absolute beam current. Calibration errors were less than 5%. Fluences ϕt and fluxes at the position of the samples were accurate to within ±10%, taking into account a possible small beam divergence. The irradiation of the glassy samples was performed us-

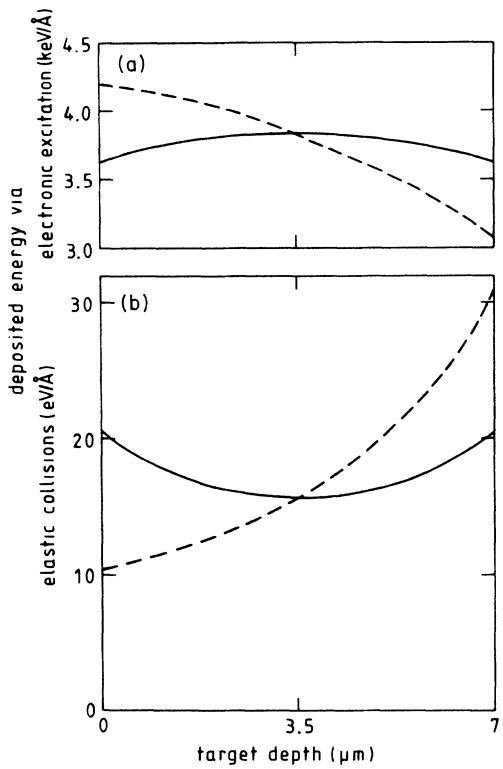

FIG. 2. Energy deposited by 360-MeV Xe ions in glassy $Pd_{84}Si_{16}$ via electronic excitations (top) and elastic collisions (bottom) as calculated by TRIM (Ref. 21) versus target depth. The total target thickness was assumed to be 7 μm. The dashed lines indicate the case without target turning. The solid lines indicate the case in which beam entrance and exit to the target are exchanged in small fluence steps.

ing fluxes between 7×10^8 and 1.5×10^9 Xe/cm^2 s.

Each irradiation run was subdivided into small fluence steps of $\phi t=10^{12}$ Xe/cm^2, with a preceding and a succeeding collimator-current calibration and a 180° turn of the samples. The turning provided the second experimental step for the improvement of the uniformity of energy deposition via S_e and S_n, respectively. The effect of turning on the depth dependence of the deposited energy is illustrated in Fig. 2 for glassy $Pd_{84}Si_{16}$. The nonuniformity of the deposited energy via S_e and S_n is less than 20% and 30%, respectively. These two values are representative for all materials of this work as can be concluded by comparing target thicknesses and projected ranges of the respective materials.

C. Irradiation temperature

As is known from earlier measurements[6,7] on glassy $Pd_{80}Si_{20}$ and $Cu_{50}Zr_{50}$ dimensional changes per unit fluence become strongly temperature dependent above about 80 K. Therefore, we aspired to maintain a low specimen temperature T during ion bombardment. Although T is an important experimental parameter, its direct determination is almost impossible because any attachment of a temperature sensor to the tiny samples wold hamper an unconstrained specimen deformation. Therefore, we have to resort to a calculation of T: The temperature of the cold stage of the cryostat was always less than 12 K during irradiation as measured with a calibrated Rh-Fe resistor. Because of the use of indium layers between samples, sample holder, and cold stage of the cryostat, it is reasonable to assume that the temperature of that portion of the specimen, which is clamped within the sample holder, is also less than 12 K. Hence, the temperaure of the outermost end of the outstanding sample part (length l) is determined by the heat input of the beam, the thermal conductivity of the sample, and l. Unfortunately, for most glasses of this work data of the low-temperature thermal conductivity λ are not available. A lower limit of the electronic part of λ can be obtained by using the Wiedemann-Franz law and an electrical resistivity of $\rho\simeq250$ $\mu\Omega$ cm, which is a high value even for metallic glasses (cf. Tables VI and VII). The phonon contribution to the thermal conductivity of glassy metals is larger than 2×10^{-3} W/cm K in the temperature range from 10 to 50 K.[19] With $\phi=1.5\times10^9$ Xe/cm^2 s, $dE/dx=S_e+S_n\simeq3.5$ keV/Å (see Fig. 2) and $l\simeq0.8$ mm, we estimate $T\leq50$ K for all materials of this work. Consequently, temperature gradients within the samples do not exceed 40 K.

D. Dimensional measurements

Before sample mounting, each sample was photographed at room temperature using an optical microscope with a magnification of 50 or 100. Subsequent to irradiation the specimens were dismounted and photographed again. For calibration purposes a slide with a 25-μm scale was used as sample support. Radiation-induced changes of sample dimensions were determined from the photons (see Fig. 3). The uncertainty of the determination of dimensional changes by this method was about ±5 μm, corresponding to a relative error about ±0.6%. Improvements of data accuracy could be obtained by averaging over numerous independent measurements. However, with increasing fluence, the relative dimensional changes of different samples of the same glass showed increasing data scattering. This behavior was due to the formation of wrinkles (see Fig. 3), which appeared in every sample because of the mechanical constraints of the sample holder and the unirradiated portion of the sample.

In the following, the expression length is used to refer to dimensional measurements in the direction from the sample holder to the outermost end of a sample, i.e., length measurements are done along the radiation-induced temperature gradient. The expression width is used to indicate dimensional measurements perpendicular to the temperature gradient (cf. also Fig. 3). A measurement of the thicknesses of the samples before and after irradiation by means of a mechanical step height monitor yielded no useful results because the nonuniformity of the sample thicknesses as well as the wrinkles introduced too large errors.

Apart from increasing data scattering, the growing wrinkles also introduced a systematic error. This error led to an underestimate of the true dimensional change because a photo reproduces only the projection of a specimen. Care was taken to keep the influence of these wrinkles small. Data points with exceptionally low values were rejected and not used in further data analysis.

E. Density measurements

Before and after irradiation, the mass density of a few samples of the glasses $Pd_{80}Si_{20}$, $Fe_{40}Ni_{40}B_{20}$, $Co_{75}Si_{15}B_{10}$, $Fe_{80}B_{20}$, and $Ni_{78}Si_8B_{14}$ has been measured at 20 °C by means of a modified flotation technique using di-iodomethane (density $D_l=3.318$ g/cm^3 at 20 °C) as the immersion liquid. Since the density of the specimens was larger than D_l and the viscosity of di-iodomethane is rather small, the samples sank down rapidly in the liquid. Therefore, on each sample a small piece of high-purity aluminum wire ($D_{\rm al}=2.698$ g/cm^3) was attached as a float, varying its mass $M_{\rm al}$ until specimen and float were floating for more than 30 min in the immersion liquid. The balance of forces yields for the density D of the samples

$$D=\frac{M_s D_l D_{\rm al}}{M_s D_{\rm al}-(D_l-D_{\rm al})M_{\rm al}}\ , \tag{1}$$

where M_s and $M_{\rm al}$ are the masses for the sample and the aluminum wire, respectively, which were determined by a microbalance.

The density of the liquid was calibrated repeatedly, using specimens of the high-purity metals Ni, Ti, Ta, and Au of known density.[20] The sensitivity of the method is predominantly limited by thermal fluctuations and convection currents within the temperature-stabilized immersion liquid. Other limiting factors can arise from a lack of chemical stability of di-iodomethane and chemical

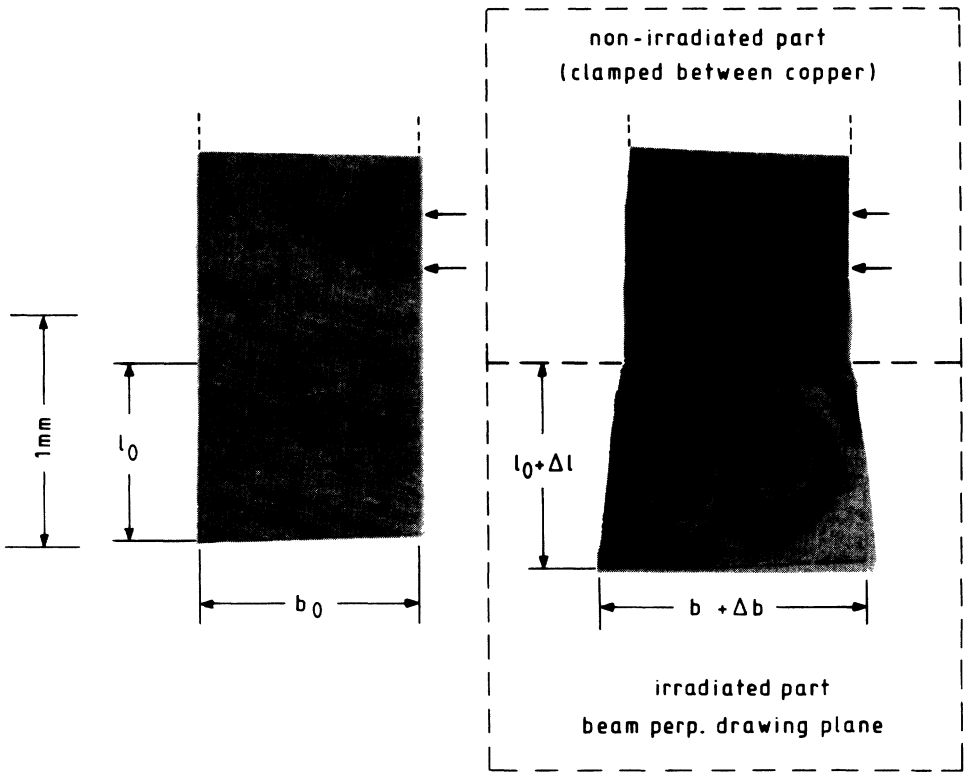

FIG. 3. Left: micrograph of a part of an unirradiated sample of glass $Co_{75}Si_{15}B_{10}$. The two arrows mark two artificial scratches, which are made to facilitate dimensional measurements. l_0 and b_0 denote length and width, respectively, of that portion of the sample which was available for exposure to the beam. Right: micrograph of the same sample, but its lower part homogeneously irradiated below 50 K with 360-MeV Xe ions up to 1.7×10^{13} cm^{-2} corresponding to about 2×10^{-3} displacement per atom (dpa). Both length and width are grown by about 15%. The bright (dark) pattern is characteristic for all irradiated specimens and is produced by wrinkles, which form during irradiation and focus (defocus) light into the objective of the microscope.

reactions between the specimen material and HI, which is a decomposition product of CH_2I_2. Nevertheless, the method is simple, applicable for tiny specimens ($\sim$400 μg) of a wide variety of materials, and accurate enough for the present purposes.

III. RESULTS

The crystalline metals and alloys did not exhibit any measurable dimensional changes after irradiation up to 1.3×10^{14} Xe/cm^2. On the contrary, during irradiation, all glassy metals investigated in this work exhibited dimensional changes both in width and length. The results of the first run are summarized in Table IV. From this table the following conclusions can be drawn.

(i) The relative changes of width b and length l are equal within the error bars. Obviously, the dimensions perpendicular to the ion beam increase homogeneously and the existing temperature gradient has no influence on the experimental results.

TABLE IV. Relative changes in width $\Delta b/b_0$ and length $\Delta l/l_0$ of glassy $Fe_{80}B_{20}$, $Ni_{78}Si_8B_{14}$, and $Co_{75}Si_{15}B_{10}$ after irradiation with 360-MeV Xe ions below 50 K.

Alloy	Pre-treatment[a]	$\phi t=2.5\times10^{13}$ Xe/cm^2 $\Delta b/b_0$ (%)	$\Delta l/l_0$ (%)	$\phi t=6\times10^{13}$ Xe/cm^2 $\Delta b/b_0$ (%)	$\Delta l/l_0$ (%)
$Fe_{80}B_{20}$	no	15.8±2.2	16.7±1.2	35.1±1.4	34.9±3.7
	yes	14.2±0.6	c	35.1±3.7	36.4±2.0
$Ni_{78}Si_8B_{14}$	no[b]	26.1±1.5	26.1±1.5	64.6±3.1	64.6±3.1
	yes	18.1±1.4	13.8±6.3	57.2±5.1	c
$Co_{75}Si_{15}B_{10}$	no[b]	29.3±1.7	29.3±1.7	62.4±6.3	72.7±3.7
	yes	24.1±1.6	24.1±2.7	72.7±3.7	77.3±2.0

[a]150 °C, 1 h in argon atmosphere.
[b]Data obtained from a linear extrapolation of low fluence data [Table VI and Eq. (2)].
[c]Data not evaluable since sample bending destroyed the well-defined irradiation geometry.

TABLE V. Summary of the density changes measured after irradiation with 360-MeV Xe ions below 50 K.

Alloy	ϕt (10^{13} Xe/cm^2)	$\Delta D/D_0$ (%)
$Pd_{80}Si_{20}$	2.0	-0.6 ± 0.5
$Fe_{40}Ni_{40}B_{20}$	0.9	-1.0 ± 0.7
$Co_{75}Si_{15}B_{10}$	2.0	-0.7 ± 0.5
$Co_{75}Si_{15}B_{10}$	6.0	0 ± 2
$Fe_{80}B_{20}$	6.0	0 ± 2
$Ni_{78}Si_8B_{14}$	6.0	0 ± 2

(ii) Even at deformation levels of more than 60%, there is no tendency toward saturation.

(iii) The ion-beam-induced dimensional changes are rather independent of the sample pretreatment. The data indicate that the deformation proceeds somewhat more slowly in annealed samples. But this effect is not dramatic and disappears largely in the scattering of the data.

The results of the density measurements are listed in Table V. Obviously, the density changes are almost negligible even at a fluence as high as 6×10^{13} Xe/cm^2 at which glassy $Ni_{78}Si_8B_{14}$ and $Co_{75}Si_{15}B_{10}$ exhibit changes in length and width of more than 60%. Therefore, the sample dimension in the beam direction must have shrunk enormously during irradiation. This conclusion was also verified qualitatively by direct measurements of the thicknesses of the samples before and after irradiation.

In Fig. 4 the relative changes of width and length of glassy $Fe_{40}Ni_{40}B_{20}$ and $Fe_{80}B_{20}$ are plotted as a function of fluence ϕt. This figure demonstrates once more the uniform expansion of these metallic glasses perpendicular to the ion beam. In addition, an almost negligible change in mass density (see Table V) again implies a considerable shrinkage of the sample in the direction of the beam.

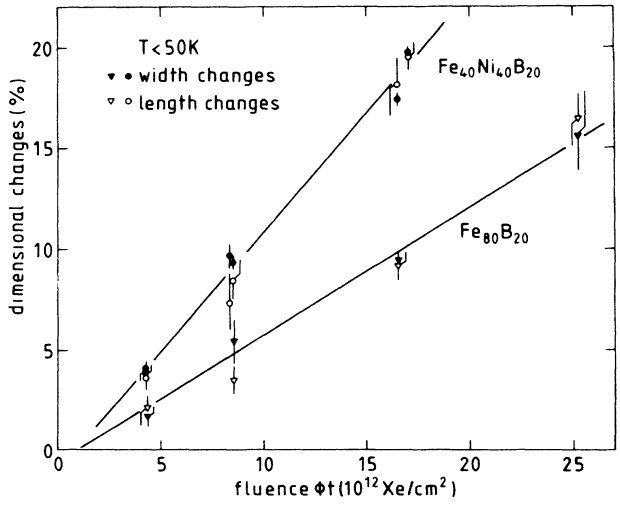

FIG. 4. Relative changes in length (open symbols) and width (solid symbols) vs fluence ϕt for glassy $Fe_{40}Ni_{40}B_{20}$ (○,●) and glassy $Fe_{80}B_{20}$ (▽,▼). Both length and width were orientated perpendicular to the beam. The straight lines are least-squares fits to the experimental data according to Eq. (2).

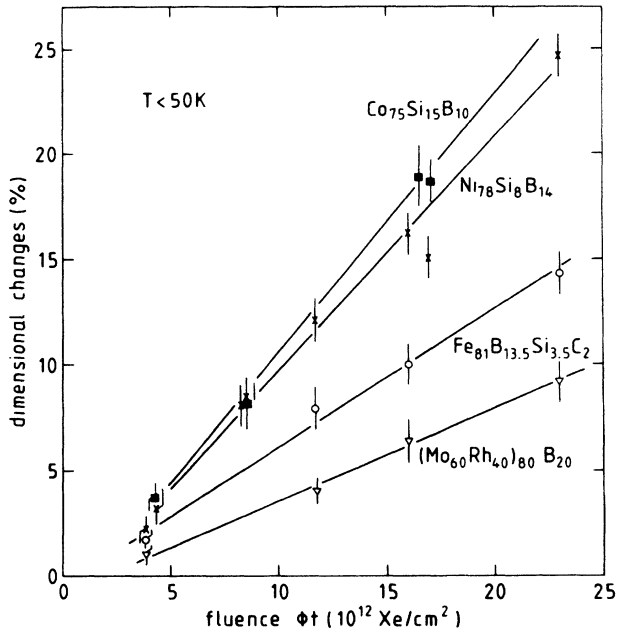

FIG. 5. Relative changes in sample dimensions for various metal-metalloid glasses irradiated below 50 K with 360-MeV Xe ions as a function of fluence ϕt. The samples were orientated perpendicular to the ion beam. The straight lines are least-squares fit to the experimental data according to Eq. (2).

In Figs. 5–8 the dimensional changes are plotted versus ion fluence ϕt for a broad variety of metallic glasses. For the sake of clarity the distinction between length and width has been dropped, because there was no detectable difference in the radiation-induced evolution of these two dimensions, within the limits of error. It is obvious from the data of Figs. 4–8 that the relative dimen-

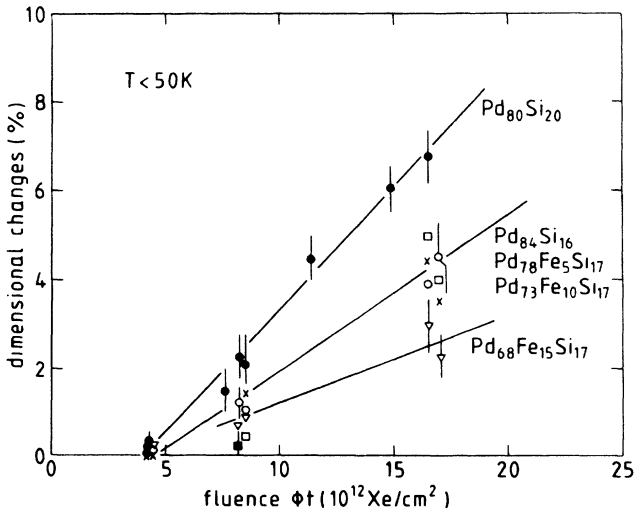

FIG. 6. Same as Fig. 5.

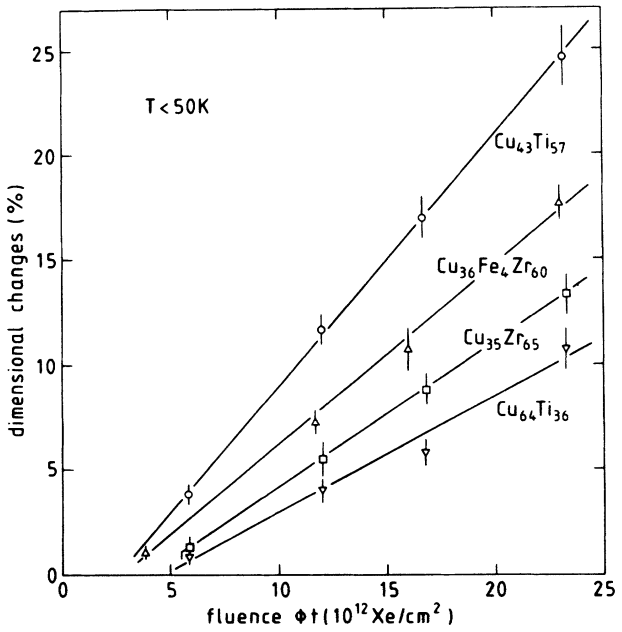

FIG. 7. Same as Fig. 5 but for various metal-metal glasses.

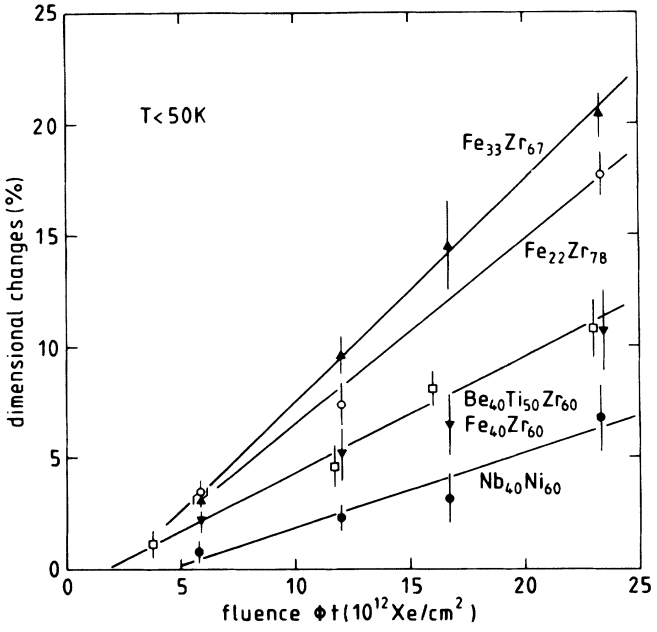

FIG. 8. Same as Fig. 7.

TABLE VI. Summary of the fit parameters A and B [see Eq. (2)] of the metal-metalloid glasses of this work. The quantity k denotes the apparent number of atoms, per unit length and projectile, which have altered their position to constitute the dimensional changes [see Eq. (7) and Fig. 9]. The electrical resistivity ρ and Young's modulus E are also included.

Alloy	A (10^{-15} cm^2)	B (10^{12} cm^{-2})	k (nm^{-1})	ρ ($\mu\Omega$ cm)	E (GPa)
$Pd_{80}Si_{20}$	5.5±0.3	4.1±0.4	75	80[a]	68[f]
$Pd_{84}Si_{16}$	3.5±0.8	4.5±2.7	48	85[b]	
$Pd_{78}Fe_5Si_{17}$	3.2±0.5	4.2±0.6	44	156[b]	
$Pd_{73}Fe_{10}Si_{17}$	3.6±0.6	5.5±0.7	50	174[b]	
$Pd_{68}Fe_{15}Si_{17}$	1.5±0.3	3.8±0.3	21	170[b]	
$Pd_{73}Co_{10}Si_{17}$	1.1±0.5	4.0±0.6	15	155[b]	
$Pd_{68}Ni_{15}Si_{17}$	1.5±0.5	4.7±0.5	21	102[b]	
$Fe_{80}B_{20}$	6.3±0.8	1.1±1.1	120	120[c]	167[e]
$Fe_{79}B_{16}Si_5$	7.8±0.6	1.4±1.1	145	125[c]	
$Fe_{78}B_{13}Si_9$	7.4±0.3	1.4±0.6	135	137[c]	157[e]
$Fe_{81}B_{13.5}Si_{3.5}C_2$	6.3±0.4	0.7±1.0	116	135[c]	
$Fe_{40}Ni_{40}B_{20}$	12.0±0.4	1.2±0.6	233	118[c]	160[f]
$Fe_{40}Ni_{38}Mo_4B_{18}$	11.0±0.9	0.6±1.2	208	138[c]	
$Ni_{78}Si_8B_{14}$	11.0±0.5	1.3±0.8	214	90[c]	137[e]
$Co_{75}Si_{15}B_{10}$	12.4±0.6	1.4±0.6	233	130[c]	149[e]
$Co_{66}Fe_4Mo_2B_{12}Si_{16}$	13.0±0.7	2.4±0.6	247	135[c]	150[c]
$Mo_{48}Rh_{32}B_{20}$	4.3±0.2	1.8±0.6	65	205[d]	

[a]Reference 23.
[b]Zhou Xinming, H. R. Khan, and Ch. J. Raub, Appl. Phys. A **34**, 167 (1984).
[c]Data obtained from data sheet of supplier.
[d]W. L. Johnson and R. A. Williams, Phys. Rev. B **20**, 1640 (1979).
[e]S. H. Wang, D. E. Polk, and B. C. Giessen, in *Proceedings of the 4th International Conference on Rapidly Quenched Metals, Sendai, Japan, 1981,* edited by T. Masumoto and K. Suzuki (The Japan Institute of Metals, Sendai, 1982), Vol. II, p. 1365.
[f]H. U. Künzi, in *Glassy Metals II,* edited by H. Beck and H. J. Güntherodt (Springer-Verlag, Berlin, 1983), p. 169.

TABLE VII. Same as Table VI but for the metal-metal glasses of this work.

Alloy	A (10^{-15} cm^2)	B (10^{12} cm^{-2})	k (nm^{-1})	ρ ($\mu\Omega$ cm)	E (GPa)
$Be_{32.5}Zr_{67.5}$	6.1±0.4	2.0 ± 1.1	65	252[a]	
$Be_{32.5}Nb_7Zr_{60.5}$	5.4±0.4	2.1 ± 1.3	59	231[a], 187[b]	
$Be_{32.5}Mo_7Zr_{60.5}$	5.4±0.4	4.0 ± 1.3	60	220[b]	
$Be_{40}Ti_{50}Zr_{10}$	5.2±0.5	1.8 ± 1.4	70	210[c]	107[c]
$Co_{22}Zr_{78}$	7.9±0.8	2.0 ± 1.6	79	163[d]	
$Cu_{35}Zr_{65}$	6.9±0.1	4.1 ± 0.5	71	166[d]	~70[f,c]
$Ni_{24}Zr_{76}$	6.0±0.8	0 ± 2	60	166[d], 158[e]	59[g]
$Fe_{22}Zr_{78}$	8.2±0.8	2.1 ± 1.5	80	163[d]	
$Fe_{33}Zr_{67}$	9.9±0.3	2.4 ± 0.5	104	168[d]	
$Fe_{40}Zr_{60}$	4.2±0.3	0.2 ± 1.1	46	170[d]	
$Fe_4Cu_{36}Zr_{60}$	8.6±0.4	3.0 ± 0.7	92		
$Fe_8Cu_{32}Zr_{60}$	8.7±0.7	2.8 ± 1.2	93		
$Fe_{16}Cu_{24}Zr_{60}$	8.6±0.8	2.4 ± 1.5	94		
$Fe_{24}Cu_{16}Zr_{60}$	10.0±0.4	2.6 ± 0.6	109		
$Cu_{64}Ti_{36}$	5.5±0.5	4.8 ± 1.0	79	183[e]	
$Cu_{43}Ti_{57}$	12.0±0.3	2.5 ± 0.4	156	188[e]	
$Nb_{40}Ni_{60}$	3.3±0.6	4.7 ± 3.1	47	151[e]	136[f]

[a]Calculated from data of R. Hasegawa and L. E. Tanner, J. Appl. Phys. **49**, 1196 (1978); Phys. Rev. B **16**, 3925 (1977).
[b]J. Goebbels, K. Lüders, H. C. Freyhardt, and J. Reichelt, Physica B+C **108B**, 1223 (1981); Nucl. Instrum. Methods **199**, 203 (1982).
[c]L. E. Tanner and R. Ray, Scr. Metall. **11**, 783 (1977).
[d]Z. Altounian and J. O. Strom-Olsen, Phys. Rev. B **27**, 4149 (1983); Z. Altounian, C. A. Volkert, and J. O. Strom-Olsen, J. Appl. Phys. **57**, 1777 (1985).
[e]B. L. Gallagher and D. Greig, J. Phys. F **12**, 1721 (1982).
[f]S. H. Wang, D. E. Polk, and B. C. Giessen, cf. footnote e in Table VI.
[g]R. W. Cochrane *et al.*, Ref. 10, p. 1083.

sional changes $\Delta x/x_0$ are fit well by a linear relation

$$\Delta x/x_0 = A(\phi t - B) , \quad (2)$$

where x_0 denotes the sample dimension before irradiation, orientated perpendicular to the ion beam, and A and B are two fitting parameters. The parameters which give the best fit to the experimental measurements are listed in Table VI and VII for the metal-metalloid and metal-metal glasses, respectively. The following conclusions can be drawn from these two tables.

(i) Although we deal with very different kinds of metallic glasses the variation in A and B is surprisingly small. In particular, there is no obvious difference between metal-metalloid glasses and metal-metal glasses.

(ii) The variation of A, which arises in a particular glass system by varying the composition, is of the same order of magnitude which appears by the variation of atomic components. This conclusion is substantiated by comparing the values of A for $Cu_{64}Ti_{36}$ and $Cu_{43}Ti_{57}$, $Fe_{22}Zr_{78}$, $Fe_{33.3}Zr_{66.7}$ and $Fe_{40}Zr_{60}$, $Pd_{80}Si_{20}$ and $Pd_{84}Si_{16}$, and $Fe_{80}B_{20}$ and $Fe_{40}Ni_{40}B_{20}$.

(iii) In contrast to the parameter A, B appears to be more characteristic for a certain class of glasses, e.g., B is about 4×10^{12} Xe/cm^2 for the Pd-based metalloid glasses and about 1×10^{12} Xe/cm^4 for the Fe-, Ni-, and Co-based metalloid glasses, whereas a value of 2.5×10^{12} Xe/cm^2 seems to be more specific for the metal-metal glasses investigated. Exceptions from this rule seem to be glassy $Cu_{64}Ti_{36}$, $Cu_{35}Zr_{65}$, $B_{32.5}Mo_7Zr_{60.5}$, and $Nb_{40}Ni_{60}$.

IV. DISCUSSION

A. General remarks

The results of the preceding section demonstrate that all metallic glasses of this work undergo, above an incubation fluence B, drastic dimensional changes when irradiated at low temperatures with fast heavy ions. This finding substantiates the conclusion that metallic glasses generally respond to ion-beam bombardment in the unique manner reported earlier for glassy $Pd_{80}Si_{20}$, $Cu_{50}Zr_{50}$, and $Fe_{85}B_{15}$,[6,7,13,14] i.e., (i) the sample dimensions perpendicular to the ion beam grow; (ii) the specimen dimension parallel to the ion beam shrinks; (iii) the anisotropy is induced by the beam and not by any intrinsic anisotropy within the samples; and (iv) the driving force for the phenomenon is the energy which the ions deposit into electronic excitations and ionizations.[11–14]

Although, in this work, no direct experiments to the latter item have been performed, indirect support can be obtained by a comparison of the number dN_g of atoms

that constitute the dimensional changes per unit fluence, with the number dN_d of atoms that are displaced via momentum transferring collisions (S_n). At constant mass density and above B, the number dN_g is given, for a rectangular sample of length l and width b, both perpendicular to the beam, by

$$dN_g = N\left[\frac{dl}{l}+\frac{db}{b}\right] . \tag{3}$$

Here, N denotes the total number of specimen atoms and dl and db are the changes in length and width per unit fluence $d(\phi t)$, respectively. Combining Eqs. (2) and (3) immediately yields

$$dN_g = 2NA\, d(\phi t) . \tag{4}$$

The total number of displaced atoms is given by

$$dN_d = NP\, d(\phi t) , \tag{5}$$

where P denotes the total cross section for displacements via elastic collisions. It can be calculated using the TRIM code,[21] provided the minimum displacement threshold energy T_d is known. For crystalline metals, T_d is of the order of 25 eV and there is evidence[22,23] that a similar value holds also for metallic glasses. For 360-MeV Xe ions and $T_d = 25$ eV, P is approximately 10^{-16} cm^2 for all glasses reported here. Hence the ratio $n = dN_g/dN_d = 2A/P$ varies from $n = 20$ for glassy $Pd_{73}Co_{10}Si_{17}$, which has the lowest A, to $n = 260$ for glassy $Co_{66}Fe_4Mo_2B_{12}Si_{16}$, which has the highest A value of the materials of this work. Both figures are much larger than unity, i.e., even for glassy $Pd_{73}Co_{10}Si_{17}$ 20 times the number of atoms which are displaced via S_n have apparently altered their positions, creating the measured dimensional changes.

One might argue that this discrepancy could arise from the use of an inadequate high value of T_d and the correct one might be much lower than 25 eV in metallic glasses due to their more open structure with respect to crystals. However, in order to obtain $n < 1$, a displacement threshold less than 1 eV is required for almost all glasses of this work. Such a low value is in serious conflict with the mechanical stability of these glasses at room temperature because the application of a moderate external stress in a material with $T_d < 1$ eV should result in observable creep by thermally activated displacements of atoms.

B. The parameter A

The parameter A has a simple physical meaning. Indeed, the relative change of sample surface $F = l \times b$ per $d(\phi t)$ is

$$\frac{1}{F}\frac{dF}{d(\phi t)} = \frac{1}{l}\frac{dl}{d(\phi t)} + \frac{1}{b}\frac{db}{d(\phi t)} = 2A . \tag{6}$$

Recognizing that $F\, d(\phi t)$ is the number dp of ions which strike the sample, we immediately arrive at the result that $2A$ is the change in specimen surface per incoming ion.

An even more informative quantity related to A can be obtained by the following consideration. The total number N of sample atoms is simply $N = N_a F t$, where t stands for the specimen thickness and N_a is the number density of atoms. Equation (4) can now be rearranged to

$$k = \frac{1}{t}\frac{dN_g}{dp} = 2N_a A . \tag{7}$$

Thus, $2A$ times N_a yields the apparent number of atoms per unit length, which have changed their position from a configuration I to a configuration II [see Fig 9(a)] for a given projectile. Of course, the situation illustrated in this figure is an extreme case. It is probably more realistic to envisage, for the atomic rearrangements, a cluster of, say, 10 to 20 atoms, all of which change their sites but perform less dramatic shifts [see Fig. 9(b)]. The values for k are listed in Tables VI and VII. They vary from 15 atoms/nm for $Pd_{73}Co_{10}Si_{17}$ to 250 atoms/nm for $Co_{66}Fe_4Mo_2B_{12}Si_{16}$, demonstrating clearly the drastic rearrangements which occur in metallic glasses in the wake of a fast heavy ion.

The driving force for these rearrangements stems from electronic excitation and ionization of the target electrons.[11–14] For 360-MeV Xe ions the mean free path between two successive excitations and/or ionizations is of subatomic size. Therefore, these excitations form a continuous cylindrical trail along the (almost straight) path of the ion. The radius R of the resulting cylinder is about 30 Å.[24] Hence, the number m of atoms per unit length in the wake of the ion is $m = N_a \pi R^2 \simeq 2000$ atoms/nm.

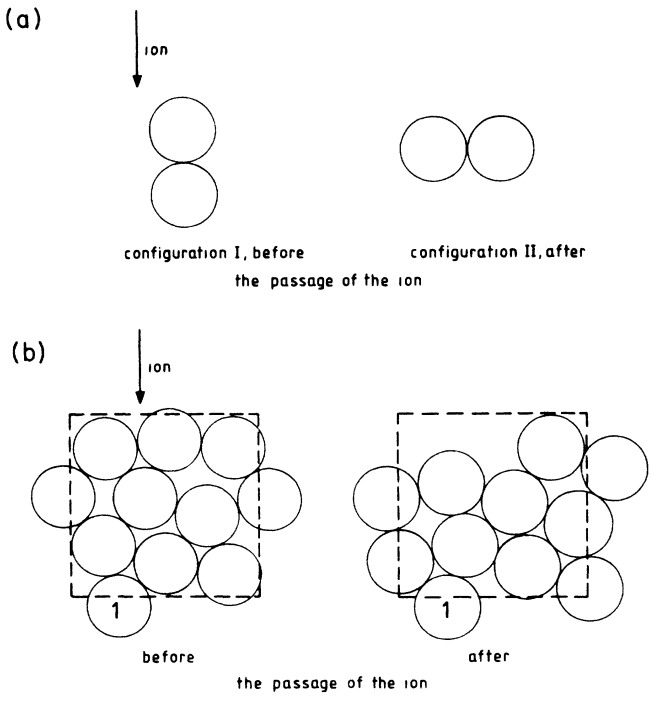

FIG. 9. (a) Idealization of an atomic rearrangement which contributes fully to the dimensional changes and involves locally only two atoms. Neighboring atoms are thought to transport the displacement field to the free sample surface via elastic interaction. (b) A more realistic picture of the occurring atomic rearrangements with a same net result as in (a).

Consequently, the ratio k/m varies from about 10^{-2} to 10^{-1}. If we take into account that atomic rearrangements are probably more like those illustrated in Fig. 9(b), we arrive at the remarkable result that a significant fraction (10–100 %) of the total number of atoms in the wake of an ion participates in the rearrangements. Whether or not the situation of Fig. 9(b) is an adequate description of this situation depends critically on the time scale on which these atomic rearrangements occur. If the latter are extremely rapid ($\sim 10^{-14}$ to 10^{-13} s), so that several transitions at a site of Fig. 9(b) can occur successively, the picture of isolated clusters may still apply. However, as soon as the atomic rearrangements proceed rather slowly ($> 10^{-12}$ s) the situation of Fig. 9(b) becomes a poor approximation and the consideration of a large number (~ 100 to 1000) of atoms performing a collective motion is more appropriate.

C. The model

From a macroscopic point of view the dimensional changes of metallic glasses proceed during ion bombardment as under the action of a mechanical stress perpendicular to the ion beam. However, the specimens do not deform like a viscous fluid. In this case, a distinct discontinuity in the sample width at the transition from the irradiated part to the unirradiated part is expected, because a viscous fluid cannot bear long-range shear stresses. In addition, a viscous sample should remain completely flat. The appearance of the characteristic wrinkles, therefore, indicates the existence of long-range elastic forces. Moreover, it is noteworthy that all fine structures visible at a specimen before irradiation can be redetected afterwards (cf. Fig. 3). Hence, the phenomenon of ion-beam-induced dimensional changes is represented macroscopically by a homogeneous plastic deformation.

On a microscopic basis, of course, the phenomenon cannot be homogeneous since it arises from individual ions. Nevertheless, it is suggestive to explain microscopically the dimensional changes as an accumulation of local plastic strains triggered by the electronically highly excited matter in the wake of the projectile. The magnitude of the local plastic strain $\varepsilon_{p,\mathrm{loc}} = \Delta R/R$ per ion is

$$\varepsilon_{p,\mathrm{loc}} = A/\pi R^2 = k/2m \tag{8}$$

since $dF/dp = 2\pi R\,\Delta R = 2A$ according to Eq. (6). For the glasses listed in Tables VI and VII, $\varepsilon_{p,\mathrm{loc}}$ varies from 5×10^{-3} to 5×10^{-2}. The appearance of strain implies the existence of a mechanical stress. Since individual ions are the origin of the strain, the essential stresses are certainly local in nature. As only matter within R of the ion's trajectory is affected, the lifetime of a local shear stress is of the order of $R/c_t \simeq 10^{-12}$ s. Here, c_t denotes the velocity for a transverse sound wave. Such a short time, however, implies an extremely high local strain rate $\dot{\varepsilon}_{p,\mathrm{loc}} \simeq 10^{10}\ \mathrm{s}^{-1}$ which, in turn, demands shear stresses which approximate the ideal shear strength $\tau_{\mathrm{id}} \simeq G/20$ of metallic glasses (G denotes shear modulus). In Ref. 25, a mechanism has been outlined which explains the rise of such high shear stresses after the passage of fast heavy ions. The basic idea is that already a radial shift of about $\Delta r/r \simeq 0.05$ of *all* atoms within R generates a shear stress $\tau \simeq G\Delta r/r \simeq G/20$, as high as τ_{id}. Such a slight shift, however, is expected to result within a few femtoseconds from the Coulomb repulsion of the ionized target atoms.[12,26] It should be added that the direction of the dimensional changes are successfully simulated by a quasistatic simulation code in which the input atomic configuration is just that which results from Coulomb repulsion.[27]

A quantitative estimate[25] of these ideas yields the following for the order of magnitude for A:

$$A = 2\pi^2 n_D R^3/\lambda_D\ , \tag{9}$$

where n_D denotes the concentration of shear sites and λ_D is the Debye wavelength which is about 2.5 Å for all metallic glasses. In deriving Eq. (9) it has been assumed implicitly[25] that the atomic rearrangements occur much faster than the duration of the shear stress. Consequently, the shear sites are envisaged to be regions with a large local free volume which makes possible an ultrafast irreversible shear transition. In other words, the large local free volume allows the shear sites to exhibit a liquidlike behavior. According to the free-volume theory of glasses,[28] n_D is expected to be somewhere between 10^{-5} and 10^{-3}, independent of the particular nature of the glass. The radius R is essentially determined by the dynamic interaction between projectile ion and target electrons and is also rather material independent. Inserting $R = 30$ Å, $\lambda_D = 2.5$ Å, and $10^{-5} \le n_D \le 10^{-3}$ we obtain

$$2\times10^{-16}\ \mathrm{cm}^2 \le A \le 2\times10^{-14}\ \mathrm{cm}^2\ . \tag{10}$$

This inequality specifies the order of magnitude of A and should hold for all glasses. Indeed, the measured values of A (cf. Tables VI and VII) are well within the range given by (10). Since there is no free volume in crystals at all, i.e., $n_D = 0$, we obtain $A = 0$ for crystalline materials which is also in agreement with the experimental results of this work.

It is important to note that the concentration n_D of shear sites is about a factor of 100 lower than the apparent concentration k/m of rearranging atoms. This means that every shear site must be a nucleus for about 100 rearrangements with the net result of Fig. 9(a). This is certainly only possible when the free volume of a shear site is not strictly localized but is distributed among a cluster of atoms [cf. Fig. 9(b)]. However, whether a shear site can allow for 100 rearrangements within about 10^{-12} s remains to be shown. An answer might be obtainable through a computer simulation using molecular dynamics. However, with regard to the time scale and the large number of atoms to be simulated, such a calculation seems to be a tedious task even for a modern high-speed computer.

Another possible explanation of the large number of rearrangements is the postulation of a previously unknown mechanism for the creation of shear sites, exceeding the preexisting number of sites by 2 orders of magnitude. This possibility has been put forward by our French colleagues, who conclude from their resistance

measurements on glassy $Fe_{85}B_{15}$ irradiated with 3-GeV Xe ions that electronic excitations and ionizations themselves create defects, providing an essential contribution to the occurrence of the dimensional changes.[13,14] It should be noted that changes in electrical resistivity induced by S_e are not in conflict with the model used above, since it claims that atomic rearrangments are indeed induced by electronic excitations. The conflict arises from the implicit assumption[13,14] that the observed resistivity changes represent a measure for the concentration of shear sites. Further experiments are necessary to clarify this point.

D. The parameter B

The physical meaning of the parameter B is obvious from Figs. 4–8: For $\phi t < B$ the dimensional changes are small and disappear within the experimental resolution. For $\phi t > B$ the dimensional changes become significant and A reaches a constant value which indicates a transition to a new steady state. Therefore, B has the meaning of an incubation fluence below which the glass is prepared to fully show ion-beam-induced plastic deformation. The transition to the new steady state should be reached when a substantial fraction of a sample volume is covered with plastically deformed regions, i.e.,

$$B \simeq (\pi R^2)^{-1} = 3.5 \times 10^{12} \text{ cm}^{-2} , \quad (11)$$

having used again $R = 30$ Å. The experimental values (cf. Tables VI and VII) are in reasonable agreement with the result of Eq. (11). It should be noted, however, that Eq. (11) is also an order-of-magnitude estimate only. A more precise evaluation of B requires a fully developed theory on ion-beam-induced plastic deformation which clearly specifies how the steady state is reached. In this context there are at least two effects which require further consideration. First, it is clear that each plastically deformed region around an ion's path must be surrounded by a residual elastic stress field. The superposition of these leads, with increasing fluence ($\phi t < B$), to a gradual mechanical polarization which certainly has some effect on the deformation rate. A correct theoretical treatment of this mechanical polarization has to include real sample surfaces, e.g., by introducing image stresses, and to consider the possibility that a linear superposition principle might not hold, i.e., close-lying deformed regions may stabilize each other by opening new paths for a relaxation of residual stress.[29]

A second effect, which might be important for a true understanding of the incubation period, concerns radiation-induced changes of the microscopic structure of a glass. To illustrate this statement we assume that the structural modifications are adequately modeled by the free-volume theory. According to the latter the concentration of shear sites is given by[30,31]

$$n_D = \exp(-\gamma v^* / v_F) , \quad (12)$$

where v_F is the average free volume per atom, v^* denotes a minimum local free volume required to trigger a shear transformation, and γ is a geometrical factor between 0.5 and 1. For metallic glasses γv^* is about 0.2 Ω and $v_F = 0.025$ Ω,[32] where Ω denotes the atomic volume. Now we assume that the irradiated glass undergoes a volume increase of 1% (cf. Table V). This implies an increase in v_F from 0.025 to 0.035 Ω, resulting in an increase in n_D from 3×10^{-4} to 3×10^{-3}. Obviously, a slight change in sample volume yields a big change in the number of shear sites. It should be pointed out that our density measurements are accurate enough to prove the anisotropy of the dimensional changes but are not accurate enough to provide reliable information concerning the concentration of shear sites. Moreover, the density of the irradiated specimens is determined at room temperature whereas the desired quantity must refer to the irradiation temperature < 50 K. Considerable structural relaxation can occur between these temperatures.[23]

E. Comparison: This model and ion-explosion spike

The model used in this work bears some resemblance to the well-known "old" ion-explosion spike.[4] This spike was originally devised to offer an explanation for the formation of nuclear tracks in solids. There are, however, two important differences between these two models. One difference concerns the time scale on which the Coulomb repulsion is active. In the ion-explosion-spike model,[4] the time scale was postulated to be of the order of a lattice vibration time, i.e., $t \simeq 10^{-13}$ s. In the model used in this work the time scale is set by the return times of the electrons in the plasma state, i.e., $t \simeq 10^{-15}$ s.[12,26] This extremely short time has several important consequences. First, the new model neither requires electron traps nor low mobility of charge carriers to separate target ions and electrons for long times. Therefore, this mechanism works in every glass, irrespective of whether it is an insulator or a metal.[25] Second, no correlation is expected between the rate of deformation, A, and the electrical resistivity. This finding is corroborated by the data of this work (see Tables VI and VII). Third, the kinetic energy, which the atoms gain during Coulomb repulsion, is, in the present model, only of the order 0.1 eV/atom.[12,26] This energy is considerably less than both the threshold energy required for the generation of Frenkel defects and the surface binding energy. Thus, this mechanism should neither contribute to production of Frenkel pairs nor to sputtering of surface atoms.[1,3,33,34] The latter part of this statement is also in accord with experiment.[35]

The other difference between the two models concerns the criterion for the occurrence of irreversible material modifications. In the ion-explosion-spike model[4] the formation of latent tracks is postulated to occur as soon as the Coulomb electrostatic stress surmounts the ideal shear strength. This criterion leads to the prediction that the formation of a track is easier the softer the material is; or, more quantitatively, there should exist a correlation between a critical ionization density, necessary for the formation of a track in a material, and its shear or Young's moduli. In the model used in this work, irreversible rearrangements are postulated to occur at shear sites as soon as the radial shift of the mutually repelling target ions approximates about 5%. A radial shift of this

amount produces a shear stress $\tau=\tau_{id}$, and the shear modulus cancels out. Thus, the deformation yield depends on the concentration of shear sites but neither correlates with the shear modulus nor with Young's modulus. The data given in Tables VI and VII are in accordance with this view. It should be noted, however, that a critical ionization density still enters into the present model. First, the ionization density must be high enough to result in a cylindrical trail of ionizations. This is necessary in order to yield a preferential direction for the Coulomb repulsion. The ionization density must also be high enough to yield a radial shift of about 5% during the time of Coulomb repulsion. Unfortunately, a reliable evaluation of this time is not currently available. But it would be astonishing if this time and, consequently, the critical ionization density would be material independent.

V. CONCLUSION

Finally, we want to point out that we did not find a correlation of the deformation yield A with the glass transition temperature, the crystallization temperature, the electron-phonon coupling constant, or the coefficient of thermal expansion at room temperature. This finding may indicate that a local temperature rise in the ion's wake does not play a dominant role for the ion-beam-induced dimensional changes. However, there exists a correlation between A and the volume which is available for structural relaxation.[15] Such a correlation is again in agreement with the ideas of the free-volume theory. On the other hand, a correlation between A and v_F demonstrates that the structural relaxation, which follows the phase of electronic excitation, has obviously a significant influence on what remains finally observable. Therefore, a conclusion from the observed yield of deformation backwards to the phase in which the electronic excitation energy is converted into atomic motion is necessarily preliminary. In this paper this phase is modeled as stress generation by mutual Coulomb repulsion of the ionized target atoms. Such a mechanism is probably the simplest one imaginable and more complicated ones cannot be ruled out at the present state of knowledge.

In conclusion, it is clear that ion-beam-induced plastic deformation is now an experimentally well-established phenomenon. There is enough evidence from this and previous[25] work that these radiation-induced dimensional changes occur virtually in any amorphous material but not in crystals. From a theoretical point of view, however, a clear understanding is still lacking and the model used in this paper is certainly as naive as the "old" ion-explosion spike of Fleischer, Price, and Walker.[4] Nevertheless, the occurrence of ion-beam-induced plastic deformation in metallic glasses has demonstrated for the first time that electronic excitations and ionization may provoke substantial atomic rearrangements, even in solids with metallic conductivity. It is worthwhile to note that such big effects have not been observed in crystalline metals so far. However, there is now growing evidence that atomic rearrangements are generated by electronic excitations in these materials as well.[36,37]

ACKNOWLEDGMENTS

Thanks are due to the VICKSI staff for their support during the irradiation experiments. We are also very grateful to Dr. H. R. Khan, Dr. J. Wecker, and Dr. R. Poerscheke, for making available their specimen material for our experiments, and we thank Dr. M. Briere for critically reading the manuscript.

*On leave from Institute of Modern Physics, Academia Sinica, Lanzhou, The People's Republic of China.

[1]W. L. Brown, in *Beam-Solid Interactions and Phase Transformations,* Vol. 51 of *Materials Research Society Symposia Proceedings,* edited by H. Kurz, G. L. Olson, and Y. M. Poate (MRS, Pittsburgh, 1986), p. 53.

[2]K. Tanimura and N. Itoh, Nucl. Instrum. Methods B **33**, 815 (1988).

[3]C. C. Watson and T. A. Tombrello, Radiat. Eff. **89**, 263 (1985).

[4]R. L. Fleischer, P. B. Price, and R. M. Walker, *Nuclear Tracks in Solids* (University of California Press, Los Angeles, 1975).

[5]R. M. Walker, Radiat. Eff. **65**, 131 (1982).

[6]S. Klaumünzer and G. Schumacher, Phys. Rev. Lett. **51**, 1987 (1983).

[7]G. Schumacher, S. Klaumünzer, S. Rentzsch, and G. Vogl, J. Non-Cryst. Solids **61/62**, 565 (1984).

[8]W. L. Johnson, in *Glassy Metals I,* edited by H. J. Güntherodt and H. Beck (Springer-Verlag, Berlin, 1981), p. 191.

[9]J. Leteurtre and Y. Quéré, in *Defects in Crystalline Solids,* edited by S. Amelinckx, R. Gevers, and J. Nihoul (North-Holland, Amsterdam, 1972), Vol. 6, pp. 25–47.

[10]S. Klaumünzer, G. Schumacher, Ming-dong Hou, and G. Vogl, in *Proceedings of the 5th International Conference on Rapidly Quenched Metals, Würzburg, Germany, 1984,* edited by S. Steeb and H. Warlimont (North-Holland, Amsterdam, 1985), Vol. I, p. 895.

[11]Ming-dong Hou, S. Klaumünzer, and G. Schumacher, Nucl. Instrum. Methods B **19/20**, 16 (1987).

[12]S. Klaumünzer, Ming-dong Hou, and G. Schumacher, Phys. Rev. Lett. **57**, 850 (1986).

[13]A. Audouard *et al.*, Europhys. Lett. **3**, 327 (1987).

[14]A. Audouard *et al.*, Europhys. Lett. **5**, 241 (1988).

[15]S. Klaumünzer, Ming-dong Hou, G. Schumacher, and Li Changlin, in *Materials Modification and Growth Using Ion Beams,* Vol. 93 of *Materials Research Society Symposia Proceedings,* edited by U. J. Gibson, A. E. White, and P.P. Pronko (MRS, Pittsburgh, 1987), p. 21.

[16]J. P. Biersack, Nucl. Instrum. Methods **182/183**, 199 (1981); Z. Phys. A **305**, 95 (1982).

[17]D. Lesueur, C. R. Acad. Sci. Paris, Ser. B **266**, 1038 (1968).

[18]A. Benyagoub and L. Thomé, Phys. Rev. B **38**, 10 205 (1988).

[19]J. R. Matey and A. C. Anderson, Phys. Rev. B **16**, 3406

(1977).
[20]*Tables of Physical and Chemical Constants,* edited by G. W. C. Kaye and T. H. Laby, 14th ed. (Longman Group, London, 1973), pp. 150–153.
[21]J. P. Biersack and L. G. Haggmark, Nucl. Instrum. Methods **174**, 257 (1980); J. F. Ziegler, J. P. Biersack, and U. Littmark, in *The Stopping and Range of Ions in Solids,* edited by J. F. Ziegler (Pergamon, New York, 1985), Vol. 1.
[22]A. Audouard, J. Balogh, J. Dural, and J. C. Jousset, Radiat. Eff. **62**, 161 (1982); D. Lesueur *et al., ibid.* **77**, 125 (1983).
[23]S. Klaumünzer and W. Petry, Phys. Lett. **87A**, 314 (1982).
[24]D. Albrecht *et al.*, Appl. Phys. A **37**, 37 (1985); E. Dartyge *et al.*, Phys. Rev. B **23**, 5213 (1981); G. Fuchs *et al.*, Europhys. Lett. **3**, 321 (1987); M. Toulemonde and F. Studer, Philos. Mag. A **58**, 799 (1988).
[25]S. Klaumünzer *et al.*, Radiat. Eff. Defects Solids **108**, 131 (1989).
[26]R. H. Ritchie and C. Claussen, Nucl. Instrum. Methods **198**, 133 (1982); R. E. Johnson and W. L. Brown, *ibid.* **198**, 103 (1982).
[27]E. H. Brandt, Cryst. Lattice Defects Amorph. Mater. **11**, 171 (1985).
[28]M. H. Cohen and G. S. Grest, Phys. Rev. Lett. **45**, 1271 (1980); G. S. Grest and M. H. Cohen, Adv. Chem. Phys. **48**, 455 (1981).
[29]A. S. Argon and L. T. Shi, Acta Metall. **31**, 499 (1983).
[30]A. S. Argon, in Ref. 10, Vol. II, p. 1325.
[31]F. Spaepen, Acta Metall. **25**, 407 (1977).
[32]P. Ramachandrarao, B. Cantor, and R. W. Cahn, J. Mater. Sci. **12**, 2488 (1977).
[33]P. K. Haff, Appl. Phys. Lett. **29**, 473 (1976).
[34]L. E. Seiberling, J. E. Griffith, and T. A. Tombrello, Radiat. Eff. **52**, 201 (1980).
[35]H. Voit, private communication.
[36]A. Iwase, S. Sasaki, T. Iwata, and T. Nihira, Phys. Rev. Lett. **58**, 2450 (1987); J. Nucl. Mater. **155-157**, 1188 (1988).
[37]A. Dunlop, D. Lesueur, and J. Dural, Nucl. Instrum. Methods B **42**, 182 (1989).

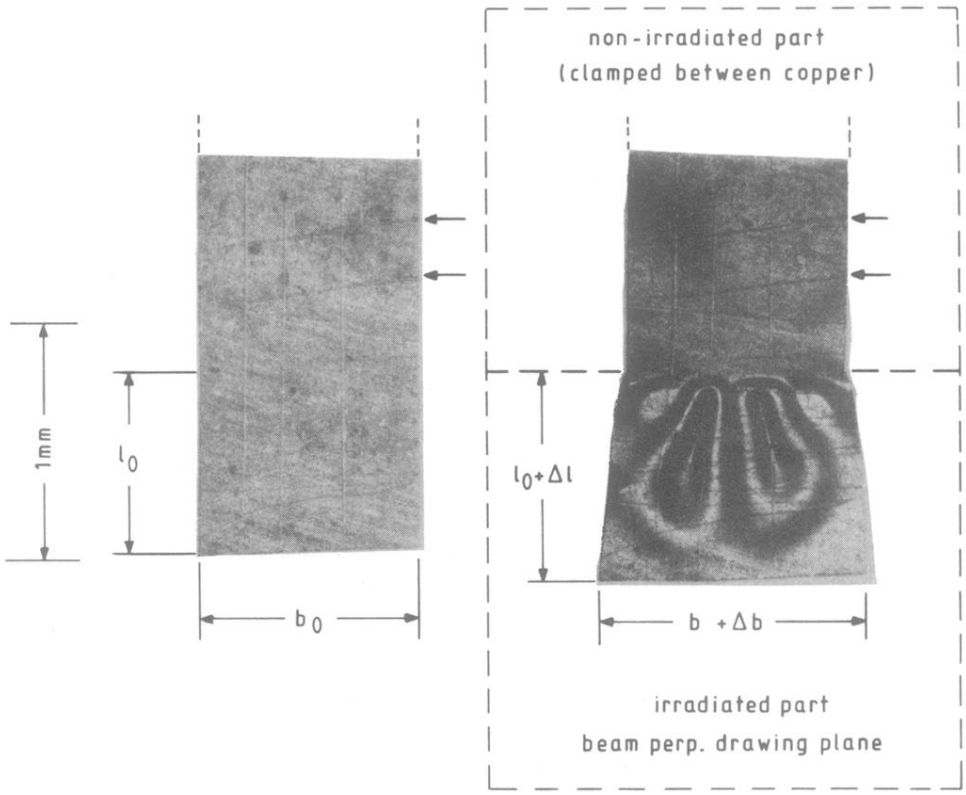

FIG. 3. Left: micrograph of a part of an unirradiated sample of glass $Co_{75}Si_{15}B_{10}$. The two arrows mark two artificial scratches, which are made to facilitate dimensional measurements. l_0 and b_0 denote length and width, respectively, of that portion of the sample which was available for exposure to the beam. Right: micrograph of the same sample, but its lower part homogeneously irradiated below 50 K with 360-MeV Xe ions up to 1.7×10^{13} cm^{-2} corresponding to about 2×10^{-3} displacement per atom (dpa). Both length and width are grown by about 15%. The bright (dark) pattern is characteristic for all irradiated specimens and is produced by wrinkles, which form during irradiation and focus (defocus) light into the objective of the microscope.